C=N stretching modes but only weak W-N stretching modes. This result is consistent with an electronic transition of strong MLCT character, as discussed above for the bpy and pyz complexes. In contrast, the resonance Raman spectrum of $W(CO)_4$(mes-dab) exhibits strong W—N stretching and ligand deformation modes, and the ligand C=N stretching modes were too weak to be detected. These observations imply that the excitation results in little transfer of charge to the mes-dab ligand π^* orbital.

In this vein, Kaim et al. have studied the ligand π^* level in a series of chelated $Mo(CO)_4L$ complexes, where L = 4,4'-bipyrimidine (bpm), 3,3'-bipyradazine (bpdz), 2,2'-bipyrazine (bpz), and 2,2'-bipyrimidine (bpym). Hückel MO calculations for these ligands have illustrated that they are π-electron deficient in the order bpm > bpz > bpym > bpdz.[31] The solvent sensitivity of these $M(CO)_4L$ complexes has been reported to closely follow this order (i.e., complexes of bpm display the most pronounced solvatochromism[32]) concordant with varying degrees of MLCT character.

Also relevant is the study by Van Eldik et al. on the piezochromic and thermochromic behavior of $Mo(CO)_4L$ complexes (L = bpy, phen, dab).[33] Observed spectral changes at elevated pressure and temperature have been shown to be associated with solvent polarity changes. An increase in solvent polarity at increasing pressure is accompanied by a blue shift in the MLCT transition, whereas a decrease in solvent polarity at increasing temperature red shifts this band.

Acknowledgment. We thank the donors of the Petroleum Research Fund, administered by the American Chemical Society, for supporting this research.

Registry No. $W(CO)_4$(bpy), 15668-66-3; $(OC)_5W$(pyz)$W(CO)_5$, 70738-71-5.

(31) Ernst, S.; Kaim, W. *Angew. Chem., Int. Ed. Engl.* **1985**, *24*, 430.

(32) Ernst, S.; Kurth, Y.; Kaim, W. *J. Organomet. Chem.* **1986**, *302*, 211.

(33) Macholdt, H.-T.; Van Eldik, R.; Kelm, H.; Elias, H. *Inorg. Chim. Acta* **1985**, *104*, 115.

Contribution from the Department of Chemistry,
The University of Houston—University Park, Houston, Texas 77004

Reversible CO Binding by $Rh_2(O_2CCH_3)_n(HNOCCH_3)_{4-n}$. A Spectroscopic and Electrochemical Investigation

M. Y. Chavan, M. Q. Ahsan, R. S. Lifsey, J. L. Bear,* and K. M. Kadish*

Received December 12, 1985

The binding constants for carbon monoxide addition to a series of dirhodium complexes of the form $Rh_2(O_2CCH_3)_n(HNOCCH_3)_{4-n}$, where n = 0, 2, 3, and 4, were determined in 1,2-dichloroethane and in acetonitrile. At room temperature, either 1:1 or 1:2 CO adducts are observed depending upon the particular combination of bridging ligands and the nature of the solvent. In addition, the stability constants of the CO adducts were found to increase with increasing number of acetamidate bridging ions in the dirhodium complex. Cyclic voltammetry was carried out for the oxidation of $Rh_2(ac)_n(acam)_{4-n}$ in acetonitrile and dichloroethane under various CO partial pressures. The value of $E_{1/2}$ for the formation of $Rh^{II}Rh^{III}$ shifted positively with increasing CO pressure. This positive shift can be associated with log K for the 1:1 CO adduct formation. A linear relationship between log K and $E_{1/2}$ for the first oxidation of $Rh_2(O_2CCH_3)_n(HNOCCH_3)_{4-n}$ under nitrogen was observed for complexes having n = 0, 1, and 2. Finally, solution infrared spectroscopy of $Rh_2(O_2CCH_3)_n(HNOCCH_3)_{4-n}CO$ species showed that the CO stretching frequencies are lowered as the number of $HNOCCH_3$ bridging ligands is increased. The lowest CO stretching frequency in this series occurs for $Rh_2(HNOCCH_3)_4CO$, which has ν_{CO} = 2028 cm^{-1}.

Introduction

The extent of π interaction between axially coordinated π-acid ligands and the rhodium(II) centers in dirhodium(II) carboxylates has been a subject of debate in recent years.[1-5] Reversible CO binding by some dirhodium complexes and infrared spectroscopic data of the CO adducts have been reported to suggest a weak π interaction.[1,2,6] However, the primary argument against any axial π interaction comes from a low-temperature crystal structure which shows that $Rh_2(O_2CCH_3)_4(CO)_2$ has unusually long Rh-C and short C-O bond lengths.[4,7]

There is no doubt that the interaction between CO and dirhodium(II) carboxylates is quite weak. At room temperature, CO adduct formation only occurs in nonbonding solvents under an atmosphere of CO. At lower CO partial pressures the CO adduct is converted to the axially uncomplexed dimer. Thus, dirhodium complexes having electron-donating bridging ligands which are stronger donors than carboxylates should more clearly demonstrate the existence of any significant π-back-donation from the dirhodium(II) center to a π acceptor axial ligand.

Recently, we reported the syntheses of dirhodium complexes that contain stronger electron-donor bridging ligands than those in dirhodium carboxylates.[8,9] These dirhodium complexes are represented as $Rh_2(ac)_n(acam)_{4-n}$ where n = 0-4, ac = $[O_2CCH_3]^-$, and acam = $[HNOCCH_3]^-$. Increasing the number of acetamidate (acam) bridging ligands on $Rh_2(ac)_n(acam)_{4-n}$ leads to an increased ease of electrooxidation, as shown in reactions 1 and 2, as well to a lowering of the $3d_{5/2}$ binding energy of the

$$Rh^{II}_2 \rightleftarrows Rh^{II}Rh^{III} + e^- \quad (1)$$

$$Rh^{II}Rh^{III} \rightleftarrows Rh^{III}_2 + e^- \quad (2)$$

neutral complex. In addition, electrochemical and XPS studies of $Rh_2(ac)_n(acam)_{4-n}$ show that the energies of the HOMO and the core electrons are raised considerably as a result of amidate binding.[8,9] Therefore, the acetamidate and acetate/acetamidate complexes should be better π donors than $Rh_2(O_2CCH_3)_4$. This was investigated in the present study, which demonstrates that $Rh_2(ac)_n(acam)_{4-n}$ complexes reversibly bind CO. At room tem-

(1) Drago, R. S.; Tanner, P. S.; Richman, R. M.; Long, J. R. *J. Am. Chem. Soc.* **1979**, *101*, 2897.
(2) Drago, R. S.; Long, J. R.; Cosmano, R. *Inorg. Chem.* **1981**, *20*, 2920.
(3) Drago, R. S.; Long, J. R.; Cosmano, R. *Inorg. Chem.* **1982**, *21*, 2196.
(4) Bursten, B. E.; Cotton, F. A. *Inorg. Chem.* **1981**, *20*, 3042.
(5) Drago, R. S. *Inorg. Chem.* **1982**, *21*, 1697.
(6) Drago, R. S.; Cosmano, R.; Telser, J. *Inorg. Chem.* **1984**, *23*, 3120.
(7) Koh, Y. B. Ph.D. Dissertation, The Ohio State University, 1979.
(8) Chavan, M. Y.; Zhu, T. P.; Lin, X. Q.; Ahsan, M. Q.; Bear, J. L.; Kadish, K. M. *Inorg. Chem.* **1984**, *23*, 4533.
(9) Zhu, T. P.; Ahsan, M. Q.; Malinski, T.; Kadish, K. M.; Bear, J. L. *Inorg. Chem.* **1984**, *23*, 2.

0020-1669/86/1325-3218$01.50/0

perature either mono- or bisadducts of CO are formed depending on the number of acetamidate ligands and/or the binding ability of the solvent.

Experimental Section

The $Rh_2(ac)_n(acam)_{4-n}$ complexes were prepared as reported previously.[9] Complexes with $n = 0$, 1, or 3 appear to have no isomers, but the complex with $n = 2$ may consist of one or more isomeric forms.[9] However, these could not be separated or separately identified since there appears to be no difference in their spectroscopic or electrochemical properties. Reagent grade dichloromethane (CH_2Cl_2), 1,2-dichloroethane ($C_2H_4Cl_2$), and acetonitrile (CH_3CN) were purchased from Aldrich. These solvents were dried over CaH_2 and freshly distilled before use. High-purity carbon monoxide and high-purity nitrogen were obtained from Linde Gas Co. Tetrabutylammonium perchlorate (TBAP) was used as supporting electrolyte and was purchased from Fluka Chemicals. This salt was recrystallized from ethanol and vacuum-oven-dried before use.

Instrumentation. Gaseous mixtures containing different proportions of CO and N_2 were passed through dirhodium solutions using Dynablender Model 8250 electronic gas-flow controllers/meters that were purchased from Matheson Gas Products. The total equilibrium gas pressure over the solution was assumed to be 1 atm, and from the ratio of the flow rates of CO and N_2 the partial pressure of CO was calculated. Partial pressures between 0.0025 and 1 atm were possible with this apparatus. Gas mixtures were passed through a bubbler containing approximately the same volume of solvent as the investigated solution, and a flow rate of about 50–60 cm^3/min was utilized to avoid losses due to evaporation.

An IBM 9430 UV–visible spectrophotometer was used to record electronic absorption spectra and to monitor the absorbances at various wavelengths. A BAS 100 electrochemical analyzer was used for electrochemical studies. This system and the electrode configuration are described in a previous publication.[8] The solution infrared spectra were recorded with variable path length solution IR cells (Wilmad) and an IBM FTIR-32 spectrometer.

Preparation of Solutions. Carbon monoxide binding by $Rh_2(ac)_n(acam)_{4-n}$ complexes was studied in 1,2-dichloroethane, dichloromethane, acetonitrile, and water. The tetraacetate, $Rh_2(ac)_4$, has reasonable solubility in nonbonding solvents such as CH_2Cl_2 or $C_2H_4Cl_2$, but the tetraamidate, $Rh_2(acam)_4$, is insoluble. Other complexes of $Rh_2(ac)_n(acam)_{4-n}$ have intermediate solubility depending on the value of n. On the other hand, all of the $Rh_2(ac)_n(acam)_{4-n}$ complexes show excellent solubility in CH_2Cl_2 or $C_2H_4Cl_2$ saturated with CO, but the complete removal of CO from solutions results in the precipitation of complexes with values of $n = 1$ and 0. All other dirhodium complexes are soluble in the absence of CO provided that their concentration is less than 0.5 mM. Because of these solubility problems, complexes where $n = 2$, 3, or 4 were prepared under a CO atmosphere after which the CO was removed by bubbling N_2 through the solution. Prolonged bubbling of nitrogen through solutions previously containing CO was carried out until no further spectral changes were observed. This was taken to signal a complete removal of CO from the solution. Thus, the study of CO binding by $Rh_2(ac)_n(acam)_{4-n}$ complexes having $n = 2$, 3, and 4 was possible in $C_2H_4Cl_2$. No solubility problems were encountered in CH_3CN or H_2O, and in these solvents the concentration of the dirhodium species was ~1 mM.

CO binding was studied at room temperature and found to be reversible in every case. Bound CO could be removed by bubbling N_2 or air through the solution. However, when $Rh_2(acam)_4$ was exposed to CO and air for several hours, especially in water, an irreversible side reaction was noticed. The side reaction could be avoided by keeping short the time of exposure of the dirhodium complex to CO. The nature of this reaction was not investigated in this study.

Results and Discussion

Formation of $Rh_2(ac)_n(acam)_{4-n}CO$ and $Rh_2(ac)_n(acam)_{4-n}(CO)_2$. The CO binding reactions of $Rh_2(ac)_n(acam)_{4-n}$ in CH_2Cl_2 and $C_2H_4Cl_2$ are given by eq 3 and 4 while eq 5 and 6 more accurately represent CO binding in CH_3CN or H_2O. In these equations, L stands for a particular combination of bridging $[(ac)_n(acam)_{4-n}]^{4-}$ ligands and S stands for the axially ligating solvent (CH_3CN or H_2O).

$$Rh_2L + CO \rightleftarrows Rh_2L(CO) \quad (3)$$

$$Rh_2L(CO) + CO \rightleftarrows Rh_2L(CO)_2 \quad (4)$$

$$Rh_2L(S)_2 + CO \rightleftarrows Rh_2L(S)CO + S \quad (5)$$

$$Rh_2L(S)CO + CO \rightleftarrows Rh_2L(CO)_2 + S \quad (6)$$

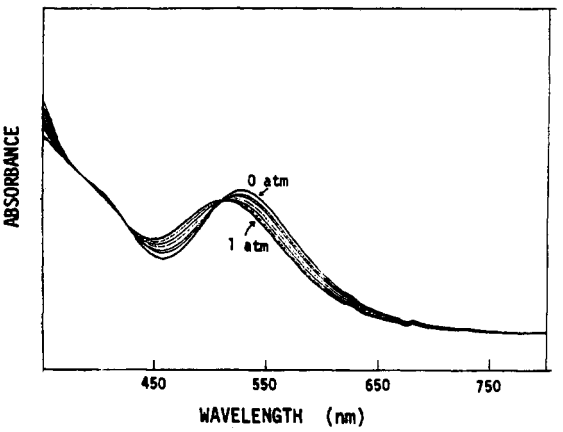

Figure 1. Changes in the visible spectra upon going from $Rh_2(ac)_2(acam)_2$ to $Rh_2(ac)_2(acam)_2CO$ in CH_3CN. The initial spectrum is in CH_3CN under N_2 (0 atm of CO) while the final spectrum was obtained in CH_3CN solutions containing 1.0 atm of CO.

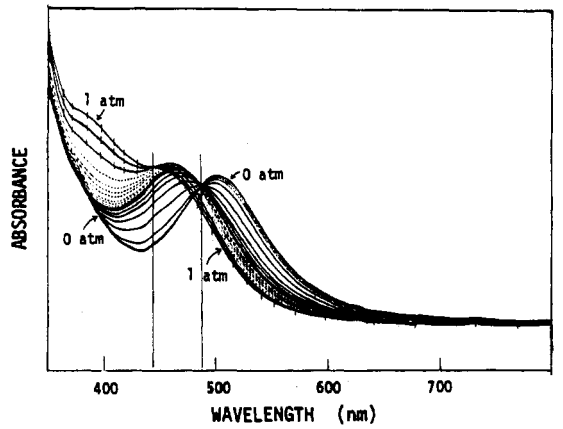

Figure 2. Changes in the visible spectra of $Rh_2(acam)_4$ in CH_3CN with increasing P_{CO}, where P_{CO} = 0.005–0.15 atm (—), 0.2–0.5 atm (---), and 0.6–1 atm (+++).

The extent to which these reactions occur depend upon the solvent and the number of acetate or acetamidate ligands. In general, as n goes to 0, an increase in the extent of CO bisadduct formation is observed. The tendency to form the CO bisadduct is also greater in nonbonding solvents where solvent molecules do not compete for the binding site. However, as mentioned in the Experimental Section, nonsolvated complexes having n values of 0 and 1 are insoluble in nonbonding solvents.

Figure 1 shows the changes that occur in the electronic absorption spectra of $Rh_2(ac)_2(acam)_2$ during the binding of CO in CH_3CN. Under a nitrogen atmosphere only one absorption peak is observed at 530 nm. As the solution is exposed to increasing partial pressure of CO, this peak diminishes and a new absorption peak appears at a shorter wavelength (~500 nm). One set of isosbestic points is observed (at 512 and 424 nm) up to a maximum CO pressure of 1 atm. The formation of the first CO adduct (reaction 5) is not complete even at 1 atm of CO. $Rh_2(ac)_4$ in $C_2H_4Cl_2$ (reaction 3) and $Rh_2(ac)(acam)_3$ in CH_3CN (reaction 5) also show similar behavior in that the formation of the monoadduct is only partially complete and no CO bisadduct is observed.

Figure 2 shows the spectral changes associated with CO binding by $Rh_2(acam)_4$ in CH_3CN. One isobestic point (at 486 nm) is observed between P_{CO} = 0–0.1 atm, and at $P_{CO} > 0.5$ atm a second isosbestic point (at 442 nm) occurs. Spectra recorded at various P_{CO} between 0.1 and 0.5 atm do not go through either of these isosbestic points, thus suggesting that equilibria 5 and 6 overlap in this range of CO pressures. The binding of CO by $Rh_2(ac)_2(acam)_2$ in $C_2H_4Cl_2$ shows similar spectral changes, and the spectra differ only in the region of partial pressures where the mono- and bisadduct formation reactions are overlapped. (These

Table I. Visible Absorption Maximum Wavelengths (λ_{max}) of Various $Rh_2(ac)_n(acam)_{4-n}$ and $Rh_2(ac)_n(acam)_{4-n}(CO)_x$ Species Where x = 1 and 2

complex	n	λ_{max}, nm ($\epsilon \times 10^{-2}$, M^{-1} cm^{-1})			$\Delta\bar{\nu} \times 10^{-3}$,[e] cm^{-1}		
		CH_3CN	$C_2H_4Cl_2$[a]	H_2O	CH_3CN	C_2H_4Cl	H_2O
$Rh_2(ac)_n(acam)_{4-n}$	4	552 (2.7)	625 (3.5)	584.3 (2.3)			
	2	528 (2.0)	618 (3.1)	572.5 (2.3)			
	1	514 (2.0)	*f*	563.3 (2.3)			
	0	500 (2.2)	*f*	555 (2.2)			
$Rh_2(ac)_n(acam)_{4-n}CO$	4	NR[g]	~540[b]	NR		2.5	
	2	~500[c,d]	530 (3.7)	*c*		2.7	
	1	473	520	495	1.68		2.5
	0	462 (1.9)	515	482	1.65		2.7
$Rh_2(ac)_n(acam)_{4-n}(CO)_2$	4	NR	NR	NR			
	2	NR	*c*	NR			
	1	*c*	385	~390		6.7	5.4
	0	~385	390	380	4.33	6.22	5.5

[a] Similar results were obtained in CH_2Cl_2. [b] Obtained under 1 atm of CO at 0 °C. [c] The reaction was incomplete at 1 atm of CO and at 0 °C. [d] See Figure 1. [e] $\Delta\bar{\nu} = \bar{\nu}_{Rh_2L(CO)} - \bar{\nu}_{Rh_2L}$ or $\bar{\nu}_{Rh_2L(CO)_2} - \bar{\nu}_{Rh_2L(CO)}$. [f] Compound insoluble in $C_2H_4Cl_2$ or CH_2Cl_2. [g] NR = no reaction at room temperature under 1 atm of CO.

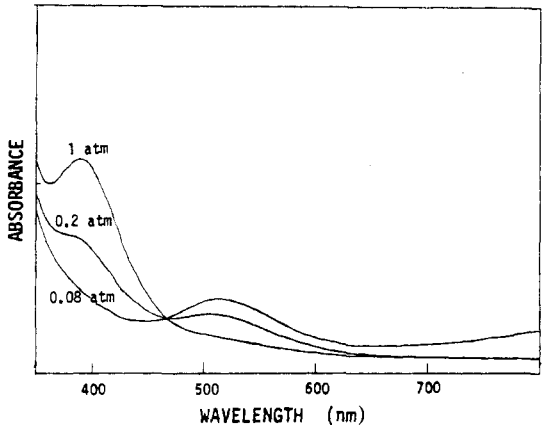

Figure 3. Electronic absorption spectra of $Rh_2(acam)_4$ in CH_2Cl_2 under various partial pressures of CO.

ligand additions are given by reactions 3 and 4 in $C_2H_4Cl_2$.)

The above two examples show spectra from which values of the binding constants can be calculated. A third category of spectra does not lend itself to the measurement of binding constants. Spectral changes of this type are shown in Figure 3 for $Rh_2(acam)_4$ in CH_2Cl_2 under various partial pressures of CO. $Rh_2(acam)_4$ is insoluble in $C_2H_4Cl_2$ or CH_2Cl_2, but the dirhodium complex dissolves as pure CO is bubbled into the solution. The spectrum recorded under P_{CO} = 1 atm shows a peak at 390 nm. As the partial pressure of CO is decreased, this peak disappears and a new peak appears at 515 nm. An isosbestic point is observed at 467 nm. The peak at 515 nm diminishes at $P_{CO} < 0.08$ atm. There are no isosbestic points below this partial pressure of CO, and at this point the complex begins to become insoluble. However, if CO is again introduced, the solution becomes clear. Because three different species (including insoluble $Rh_2(acam)_4$) are present at different CO partial pressures, the peaks at 390 and 515 nm are attributed to the 1:2 and 1:1 CO adducts, respectively.

Table I lists the wavelengths of maximum absorption (λ_{max}) for the $Rh_2(ac)_n(acam)_{4-n}$ complexes with and without bound CO. In many cases the λ_{max} values in the presence of CO are only approximate (±3 nm) since an accurate identification of peak wavelength is complicated by overlapping equilibria or incomplete reactions. However, a few observations may be made from the data in Table I. First, the spectral maxima of $Rh_2(acam)_4$ and $Rh_2(acam)_4CO$ vary as a function of solvent but those for $Rh_2(acam)_4(CO)_2$ are relatively insensitive to changes in solvent. In addition, the difference in wavenumbers between a given $Rh_2(ac)_n(acam)_{4-n}$ and $Rh_2(ac)_n(acam)_{4-n}CO$ complex is ~2.6 × 10^3 cm^{-1} in CH_2Cl_2, $C_2H_4Cl_2$, and H_2O, but this difference is ~1.7 × 10^3 cm^{-1} in CH_3CN. Although the data are insufficient for a generalization, these differences appear to be relatively insensitive to the particular combination of ac and acam bridging ligands.

Table II. CO Binding Constants for $Rh_2(ac)_n(acam)_{4-n}$ Complexes in CH_3CN and $C_2H_4Cl_2$

solvent	n	log K_1 (atm^{-1})[a]			$P_{1/2}$,[b] atm
		I[c]	II[c]	III[c]	
CH_3CN	4	NR[f]	NR	NR	NR
	2	0.08 ± 0.01	NA[e]	~0.1	0.83
	1	0.68 ± 0.03	NA	0.75 ± 0.05	0.21
	0	1.51 ± 0.05	1.53	1.56 ± 0.02	0.03
C_2H_4Cl	4	0.06 ± 0.01	NA		0.87
	2	2.08 ± 0.02	2.10		0.008
	1	*d*	*d*	*d*	*d*
	0	*d*	*d*	*d*	*d*

[a] For CO binding according to eq 3. [b] $P_{1/2} = 1/K_1$ when $[Rh_2L(CO)]/[Rh_2L] = 1$. Values reported were calculated from log K_1 by using the data for I. [c] I: obtained from eq 7. II: obtained from the method in ref 2. III: obtained from electrochemical data. [d] The dirhodium complex is insoluble in $C_2H_4Cl_2$ and CH_2Cl_2 in the absence of CO; thus, K_1 cannot be determined. [e] NA: method not applicable for this system. [f] NR: no CO binding detected at room temperature.

Spectroscopic Calculation of CO Binding Constants. Only spectral changes of the type shown in Figures 1 and 2 can be used for the measurement of binding constants. For CO binding by $Rh_2(ac)_2(acam)_2$ in CH_3CN (Figure 1), a value of A_∞ for $Rh_2(ac)_2(acam)_2CO$ is not available since this complex is not fully formed at the highest investigated CO pressures. However, in such cases, a form of the Ketelaar equation[10] (eq 7) can be used

$$\frac{1}{A - A_0} = \frac{1}{K_{CO}P_{CO}C_0\Delta\epsilon} + \frac{1}{C_0\Delta\epsilon} \qquad (7)$$

to determine K_1 for formation of the monoadduct. This equation is obtained by manipulating the simple equilibrium expression $K_{CO} = [Rh_2L(CO)]/[Rh_2L][P_{CO}]$. In eq 7, C_0 is the total concentration of Rh_2L and $\Delta\epsilon$ is the difference between the molar absorptivities of Rh_2L and $Rh_2L(CO)$ at a given wavelength.

Plots of $(A - A_0)^{-1}$ vs. P_{CO}^{-1} give K_{CO} values. This was done at two different wavelengths by using a linear least-square analysis of the data. Values of K_1 are listed in Table II, where equilibrium constants are reported as atm^{-1}. Points having $1/P_{CO} < 50$ were calculated from the spectra in the region of overlapping equilibria by utilizing the method described in ref 2. In order to keep the same units in the equilibrium constants (for the sake of comparison), the CH_3CN concentration is ignored.

A method of data treatment for cases of overlapping consecutive equilibria has been discussed by Drago and co-workers.[2] This method takes advantage of the fact that a second set of isosbestic points is observed at higher P_{CO} values. For the particular case of $Rh_2(acam)_4$ in CH_3CN, the second isosbestic point occurs at

(10) Rose, N. J.; Drago, R. S. *J. Am. Chem. Soc.* **1959**, *81*, 6138 and references therein.

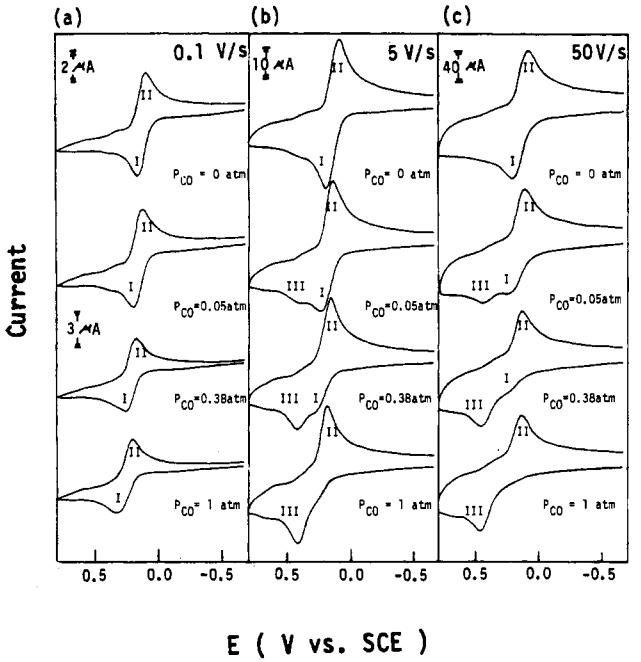

Figure 4. Cyclic voltammograms of $Rh_2(acam)_4$ in CH_3CN (0.1 M TBAP) under various N_2 and CO atmospheres at sweep rates of (a) 0.1 V/s, (b) 5 V/s, and (c) 50 V/s.

442 nm. The absorbance at this isosbestic point gives the molar absorptivity of the 1:1 adduct (ϵ_1), and the molar absorptivity for free $Rh_2(acam)_4$ at 422 nm (ϵ_0) is obtained from the initial spectrum in the absence of CO. Spectra were recorded under various CO partial pressures and the absorbance of the nonisosbestic spectral points at 442 nm was used to calculate the corresponding Rh_2L or $Rh_2L(CO)$ concentrations. Only spectra passing through the first isosbestic point were used in the calculation. The Rh_2L concentrations thus obtained were in turn used to calculate ϵ_1 at other nonisosbestic wavelengths from the spectra passing through the first isosbestic point. The ϵ_1 values thus obtained varied within ±1%. An A_∞ value for 1:1 adduct formation was obtained from the averaged ϵ_1 value.

The exact equations used in the calculation of K_{CO} are given in ref 2. In the present study, K_{CO} was calculated from a plot of log $[(A_\infty - A)/(A - A_0)]$ vs. log P_{CO}. The K_{CO} value obtained from two different wavelengths was found to agree within 5% of the value obtained by using the Ketelaar equation. log K_{CO} values are listed in Table II. Table II also lists the $P_{1/2}$ values where $P_{1/2}$ is the CO partial pressure for which $Rh_2L/Rh_2L(CO) = 1$.

Electrochemistry of $Rh_2(acam)_4$ in CH_3CN Containing CO. The electrooxidation of $Rh_2(acam)_4$ was investigated in CH_3CN as a function of potential scan rate and CO pressure. This type of data are shown in Figure 4. Under an N_2 atmosphere (P_{CO} = 0 atm) only one oxidation and one rereduction peak are observed. At 0.1 V/s (Figure 4a) these peaks are separated by 60–70 mV, but at a faster scan rate of 50 V/s this peak to peak separation is ~120 mV. However, a plot of i_p vs. $v^{1/2}$ is linear, indicating a diffusion-controlled one-electron oxidation.

The CO pressure was increased from 0 to 1 atm and the oxidation carried out at a number of scan rates that varied between 0.1 and 50 V/s. At 0.1 V/s, an increase in CO pressure resulted in a positive shift of the first oxidation/reduction process (labeled peaks I and II in Figure 4). This shift is shown in Figure 5, which correlates $E_{1/2}$ with log P_{CO} at 0.1 V/s. As seen in this figure, there are three different regions of voltammetric behavior. At log P_{CO} values between −2.39 and −1.82, peaks I and II are invariant with increase in CO pressure, indicating the occurrence of only reaction 1. From a log P_{CO} value of −1.69 to −0.2, $E_{1/2}$ shifts by +57 mV/10-fold change in P_{CO}. At log $P_{CO} > -0.2$ a third relationship is observed and the slope increases to about 105 mV/10-fold increase in P_{CO}.

The CO partial pressure at which this third segment commences (0.6 atm) compares very well with the P_{CO} at which the visible

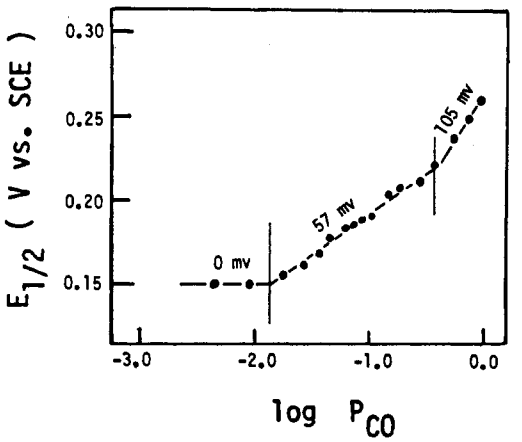

Figure 5. Correlation between $E_{1/2}$ and log P_{CO} for $Rh_2(acam)_4$ oxidation (reaction 1) at 0.1 V/s in CH_3CN containing 0.1 M TBAP.

Scheme I

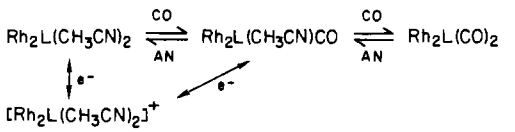

spectra of $Rh_2(acam)_4$ begin to pass through the second isosbestic point in Figure 2. In this region, the anodic (oxidation) peak shifts positively more than the cathodic (reduction) peak with increase in P_{CO} (see Figure 4a), and as such, the apparent $E_{1/2}$ value is no longer a true thermodynamic value. However, a plot of cathodic peak II vs. log P_{CO} does show a 59-mV shift at all CO pressures up to log $P_{CO} = 0$. This suggests that the oxidation and reduction processes are not coupled above a CO pressure of 0.6 atm and that at these pressures two different electron-transfer pathways are observed in the oxidation and in the reduction. This indeed is the case, as illustrated by the cyclic voltammetric curves at 5 V/s (Figure 4b) and 50 V/s (Figure 4c). As seen in these voltammograms, the combination of high scan rates and high CO pressures leads to the appearance of a second oxidation peak (labeled peak III) as peak I disappears. At all CO pressures and scan rates only a single reduction (peak II) is present.

The positive slope of 57 mV/log P_{CO} in Figure 5 and the spectroscopic data show formation of $Rh_2(acam)_4CO$ and suggest that reaction 8 occurs during electrooxidation of $Rh_2(acam)_4CO$ in CH_3CN.

$$Rh_2(acam)_4(CH_3CN)CO + CH_3CN \rightleftarrows [Rh_2(acam)_4(CH_3CN)_2]^+ + CO + e^- \quad (8)$$

A theoretical basis for the 57-mV shift in $E_{1/2}$ is given in the literature[11,12] and agrees with the loss of one CO molecule upon electrooxidation. A log K_1 value of 1.50 for the formation of $Rh_2(acam)_4CO$ is obtained from the data in Figure 5, and this value compares well with the spectroscopically calculated log K_1 = 1.56 (see Table II).

The combined electrochemical and spectroscopic data lead to the overall oxidation/reduction mechanism shown in Scheme I, where L = $(acam)_4$. The kinetics associated with loss or gain of CO in this scheme can be understood by the data in Figure 4. Peak III in Figure 4c is relatively insensitive to an increase in P_{CO} and shifts from E_p = 0.245 V at P_{CO} = 0.05 atm to E_p = 0.260 V at P_{CO} = 1 atm. However, peak II shifts from 0.084 V under N_2 to 0.145 V at P_{CO} = 1 atm. Thus, the overall shift of this cathodic peak is 35–40 mV/log P_{CO}.

The potential of peak III is also dependent on the potential sweep rate, and E_p shifts positively by approximately 40 mV/10-fold increase in scan rate. The theoretical shift of E_p is 30

(11) Galus, Z. *Fundamentals of Electrochemical Analysis*; Ellis Harwood: New York, NY, 1976; pp 360–379.
(12) Crow, D. R. *Polarography of Metal Complexes*; Academic: London, 1969.

Scheme II

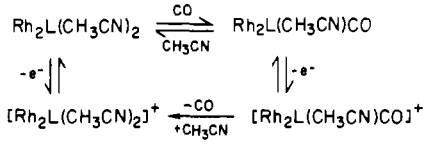

mV/log (scan rate) for a chemical reaction following electron transfer (an EC mechanism),[13] but since some IR loss is present at higher scan rates, the experimentally observed 40-mV shifts can be considered consistent with the theoretical predictions.

The spectroscopic data (Figure 2) suggest that $Rh_2(acam)_4(CH_3CN)_2$ and $Rh_2(acam)_4(CH_3CN)CO$ are mainly present under conditions of the electrochemical experiment. Although some $Rh_2(acam)_4(CO)_2$ is formed in small amounts at $P_{CO} > 0.6$ atm, a CO molecule appears to dissociate before oxidation. Also, since there is no reduction peak directly coupled to peak III, this suggests that $[Rh_2(acam)_4(CH_3CN)_2]^+$ is the only species reduced. Under these conditions the electrode reactions at all CO pressures can be illustrated by Scheme II.

The binding of CO to $Rh_2L(CH_3CN)_2$ will shift the oxidation potentials positively such that $E_{1/2}$ (or E_p) for $Rh_2L(CH_3CN)_2$ oxidation is more favorable than that of $Rh_2L(CH_3CN)CO$. Thus, one can envision a dissociation of CO prior to electron transfer and an oxidation that proceeds via $Rh_2L(CH_3CN)_2$. This dissociation appears to occur at slow scan rates, as shown in Figure 4a. However, as the scan rate is increased, the direct oxidation of $Rh_2L(CH_3CN)CO$ can also occur (see Figure 4b). Finally, at 50 V/s, the dissociation of CO prior to oxidation will become minimal and, and under these conditions, the direct conversion of $Rh_2L(CH_3CN)CO$ to $[Rh_2L(CH_3CN)CO]^+$ will predominate as the electrooxidation reaction. These conditions give rise to cyclic voltammograms of the type shown in Figure 4c at 50 V/s. As seen in this voltammogram, peak I has completely disappeared and only peak III is observed on oxidation.

Two points are of importance in Scheme II. The first is that the oxidized complex does not seem to form stable CO adducts. Although oxidation peak III appears to involve a transient CO complex, $[Rh_2L(CH_3CN)_2]^+$ is invariably the ultimate oxidized species. This species is rereduced to $Rh_2L(CH_3CN)_2$ (peak II) under all of the investigated experimental conditions, but in the presence of CO the mono- or bisadduct is formed in solution after the electron transfer (an electrochemical EC mechanism). All of these data indicate that a thermodynamic half-wave potential for the conversion of $Rh_2L(CH_3CN)CO$ to $[Rh_2L(CH_3CN)CO]^+$ cannot be measured in CH_3CN. This is due to the strong binding of CH_3CN by the oxidized complex. Such solvent binding does not occur in CH_2Cl_2, and in these cases the $E_{1/2}$ value for this reaction may be obtained. This is discussed in the following section.

Electrochemistry of $Rh_2(acam)_4$ in CH_2Cl_2 under CO. Figure 6 shows cyclic voltammograms of $Rh_2(acam)_4$ at 5 V/s in CH_2Cl_2 (0.1 M TBAP) under various CO partial pressures. Trace 1 was recorded under 1 atm of CO. Traces 2–5 were recorded under progressively smaller CO pressures. This was achieved by bubbling pure N_2 through the CO-saturated solution in short bursts. As the CO pressure decreased, the solution color changed from golden yellow to magenta. If pure N_2 was passed through the solution after trace 5 was recorded, the solution became turbid, indicating precipitation of $Rh_2(acam)_4$. (This property was discussed in an earlier section of the paper.) From the data in Figure 3, it can be estimated that the P_{CO} varied from 1 atm (Figure 6, trace 1) to ~0.08 atm (Figure 6, trace 5) during the experiment.

The anodic peak in trace 1 is labeled as peak a'_1. This peak occurs at $E_p = 0.75$ V in CH_2Cl_2 under 1 atm of CO and shifts in a negative direction with a decrease in the CO pressure. Peak a'_1 does not shift after trace 3, and the new peak is labeled as peak a_1 in traces 4 and 5. This peak, a_1, decreases in magnitude while a new peak (labeled peak a_2) appears at ~0.4 V. At the same

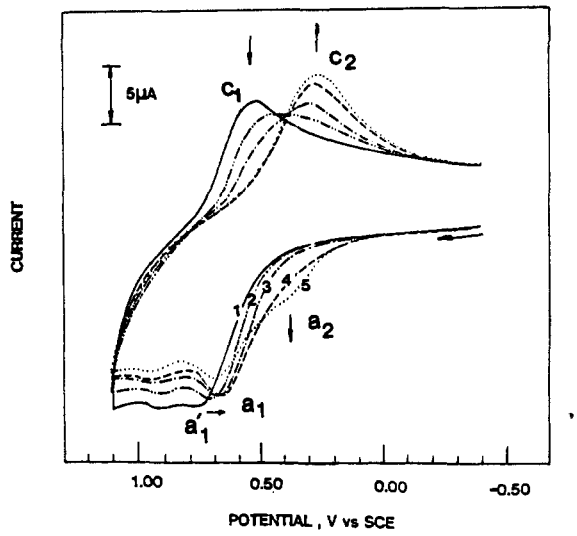

Figure 6. Cyclic voltammograms of $Rh_2(acam)_4$ in CH_2Cl_2 (0.1 M TBAP) under various CO pressures. All voltammograms were recorded at 5 V/s. Curve 1 was at $P_{CO} = 1$ atm while curves 2–5 were recorded at progressively lower values of P_{CO}.

Scheme III

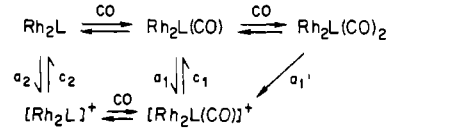

time, the initial rereduction peak in trace 1 (peak c_1 at $E_p = 0.57$ V) decreases in magnitude while a new peak appears at ~0.3 V. This peak is labeled as peak c_2 and appears to be directly coupled to peak a_2 ($\Delta E_p \sim 80$ mV). Similarly, peak c_1 appears to be coupled to peak a_1 ($\Delta E_p \sim 80$ mV) and not to a'_1. These changes with change of CO pressure can be accounted for by the oxidation–reduction mechanism shown in Scheme III.

In Scheme III, peaks c_1 and c_2 represent the reduction of $[Rh_2L(CO)]^+$ and $[Rh_2L]^+$ while peaks a_1 and a_2 represent the oxidation of $Rh_2L(CO)$ and Rh_2L. Peak a'_1 is not coupled to a reverse peak and appears to involve the oxidation of $Rh_2L(CO)_2$ to $[Rh_2L(CO)]^+$.

As seen in Figure 6, the binding of CO results in a positive shift of the $Rh_2(acam)_4$ oxidation potentials. This implies that CO binding lowers the HOMO of the $Rh_2(acam)_4$ species. It is also interesting to note that the difference in $E_{1/2}$ between the oxidation of $Rh_2(acam)_4CO$ and that of $Rh_2(acam)_4$ is ~0.27 V in CH_2Cl_2. The increase in energy of the visible absorption bands on going from $Rh_2(ac)_n(acam)_{4-n}$ to $Rh_2(ac)_n(acam)_{4-n}CO$ in CH_2Cl_2 (Table II) is $\sim 2.5 \times 10^3$ cm^{-1}, $\simeq 0.3$ V. This similarity may not be purely fortuitous.

Electrode Reactions of $Rh_2(ac)_n(acam)_{4-n}$ and Correlations between $E_{1/2}$ and CO Formation Constants. Electrochemical results similar to those discussed above were obtained for $Rh_2(ac)_n(acam)_{4-n}$ complexes having $n = 1$ and 2 in CH_3CN and for complexes having $n = 2$ and 4 in CH_2Cl_2. However, the positive shift of potential for the oxidation peak was small (~40 mV) or did not occur under 1 atm of CO for complexes with higher values of n in CH_3CN. For example, $Rh_2(ac)_4$ in CH_3CN showed no shift of potential upon exposure to 1 atm of CO while a small positive shift of potential was observed for the same complex under 1 atm of CO when CH_2Cl_2 was the solvent. In a given solvent system, K_1 for the addition of one CO increased as the number of acam ligands in $Rh_2(ac)_n(acam)_{4-n}$ increased. This is seen from Table II and is shown graphically in Figure 7, which shows the relationship between log K_1 and $E_{1/2}$ of $Rh_2(ac)_n(acam)_{4-n}$. A linear relationship with a slope of 3.0 log units/V is obtained for complexes where $n = 0$–2 in CH_3CN. In $C_2H_4Cl_2$, only two points are available ($n = 2$, 4) and an approximate slope of 3.7 log units/V is estimated from these two points. On the basis of these correlations, a log K_1 value of −1.4 ($K_1 = 0.04$ atm^{-1}, $P_{1/2} = 25$

(13) Nicholson, R. S.; Shain, I. *Anal. Chem.* **1984**, *36*, 706.

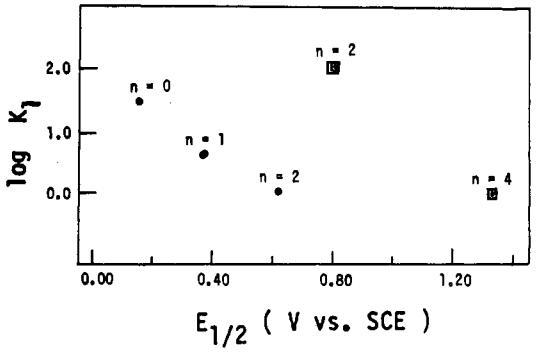

Figure 7. Correlation between log K_1 for CO binding to $Rh_2(ac)_n(acam)_{4-n}$ and $E_{1/2}$ for reaction 1 in (●) CH_3CN (0.1 M TBAP) and (⊡) $C_2H_4Cl_2$ (0.1 M TBAP).

atm) may be predicted for $Rh_2(ac)_4$ in CH_3CN, consistent with the fact that $Rh_2(ac)_4$ shows no detectable CO binding in CH_3CN. Similarly, the log K_1 value for $Rh_2(acam)_4CO$ formation in CH_2Cl_2 or $C_2H_4Cl_2$ may be expected to be ~3.7 ($K_1 \sim 5 \times 10^3$, $P_{1/2} = 2 \times 10^{-4}$ atm).

Infrared Spectroscopy. A stretching frequency of 2095 cm^{-1} has been reported for CO bound to $Rh_2(O_2CC_3H_7)_4$,[3] but it is not clear if this frequency represents the 1:1 or the 1:2 CO adduct. A lowering of the CO stretching frequency from 2143 cm^{-1} for free CO to 2095 cm^{-1} for the CO adduct of $Rh_2(O_2CC_3H_7)_4$ has been used to support the hypothesis of π-back-donation from the dirhodium ions to bound CO. However, it has been suggested[4] that there is an inconsistency between the IR data and the Rh–C and the C–O bond lengths obtained from a low-temperature crystal structure of $Rh_2(ac)_4(CO)_2$.[4,7] The IR data support π-back-donation while the bond lengths contradict it.

The IR data for CO-bound $Rh_2(ac)_n(acam)_{4-n}$ complexes in the present study strongly support the hypothesis of π-back-donation.[14] In the absence of CO no peaks are observed in the carbonyl stretching region, but under a CO atmosphere either one or two peaks are recorded.

Figure 8 (trace i) shows the room-temperature solution IR spectrum of $Rh_2(acam)$, which was dissolved in freshly distilled dry CH_2Cl_2 saturated with CO. Under these conditions the solution contains mostly $Rh_2(acam)_4(CO)_2$ (see Figure 3), and this compound is characterized by a peak at 2046 ± 1 cm^{-1}. As N_2 is bubbled through this solution, the color changes from yellow to orange-yellow to magenta. Traces ii–iv show changes in the IR spectra during this progression. As N_2 passed through the solution, the peak at 2046 cm^{-1} diminishes while another peak appears at 2028 ± 1 cm^{-1}. By correlation with visible spectroscopic data (Figure 3), the former peak (2046 cm^{-1}) is attributed to $Rh_2(acam)_4(CO)_2$ and the latter (2028 cm^{-1}) to $Rh_2(acam)_4CO$.

The 1:1 and 1:2 CO adducts of other $Rh_2(ac)_n(acam)_{4-n}$ complexes could not be distinguished from one another by IR spectroscopy. For the complex with $n = 1$, a peak is observed at 2059 cm^{-1} under ~1 atm of CO, and as N_2 is passed into solution, this

(14) The room-temperature crystal structure of $Rh_2(PhC(NPh)_2)_4CO$, where $PhC(NPh)_2$ = *N,N'*-diphenylbenzamidine, has been obtained. The Rh–C and C–O bond distances are respectively 1.97 and 1.151 Å, consistent with the hypothesis of π-back-donation. A full description of this structure will be published elsewhere.

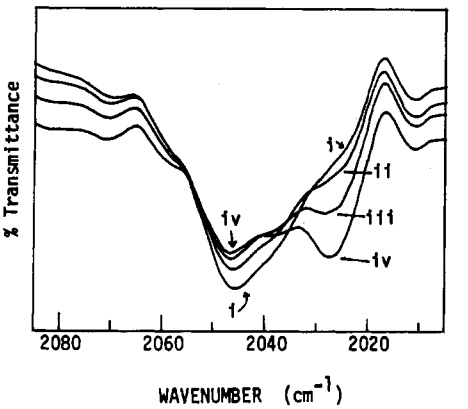

Figure 8. Infrared spectra of $Rh_2(acam)_4(CO)_x$ (x = 1 or 2) in CH_2Cl_2 as a function of decreasing CO pressures from (i) $P_{CO} \simeq 1$ atm to (iv) $P_{CO} \ll 1$ atm.

peak seems to shift to 2055 cm^{-1}. A peak is observed at 2070 cm^{-1} for the complex with $n = 2$ under $P_{CO} \simeq 1$ atm, but no new peak is observed before the disappearance of this peak (as pure N_2 is bubbled in). The above data suggest that the observed IR peaks are due mainly to 1:1 CO adducts for complexes having $n = 1$ and 2. 1:2 adducts may be present at high values of P_{CO}, but the peaks for these two species may be too close to be resolved.

The ease of the metal-centered oxidation for $Rh_2(ac)_n(acam)_{4-n}$ is determined by the amount of electron density at the dirhodium center and depends upon the value of n as follows:[8,9] $Rh_2(acam)_4$ > $Rh_2(ac)(acam)_3$ > $Rh_2(ac)_2(acam)_2$. The value of ν_{CO} in metal carbonyls is known to depend inversely upon the amount of electron density back-donated from the metal to CO. In the present case, the order of ν_{CO}'s for the 1:2 or the 1:1 CO adducts is $Rh_2(ac)_2(acam)_2$ > $Rh_2(ac)(acam)_3$ > $Rh_2(acam)_4$. This is exactly opposite to the ordering based on the amount of electron density at the dirhodium center. Thus, these correlations are consistent with π-back-donation, which appears to increase with an increasing number of acam ligands in $Rh_2(ac)_n(acam)_{4-n}$.

The lowering of ν_{CO} upon going from $Rh_2(acam)_4(CO)_2$ to $Rh_2(acam)_4CO$ is noteworthy and may be explained on the basis of π-back-donation. In $Rh_2(acam)_4(CO)_2$ the two CO's must "share" the electron density on the Rh–Rh π^* orbital(s) while this is not the case for $Rh_2(acam)_4CO$. The bound CO in $Rh_2(acam)_4CO$ may thus receive more electron density than the CO's in $Rh_2(acam)_4(CO)_2$, and this would lead to the difference in ν_{CO} of each reported above.

In summary, the spectroscopic and electrochemical measurements reported in this paper are all consistent with the hypothesis that π-back-bonding occurs in CO adducts of $Rh_2(ac)_n(acam)_{4-n}$ and that the degree of π-back-bonding increases as n goes from 4 to 0.

Acknowledgment. We wish to thank the Robert A. Welch Foundation (J.L.B., Grant No. E-918, and K.M.K., Grant No. E-680) for financial support for this work. Thanks are also due to X. Q. Lin for his help in recording some of the electrochemical data.

Registry No. $Rh_2(HNOCCH_3)_4$, 87985-40-8; $Rh_2(OAc)_2(HNOCCH_3)_2$, 87985-38-4; $Rh_2(OAc)_3(HNOCCH_3)$, 87985-37-3; $Rh_2(OAc)_4$, 15956-28-2; $Rh_2(HNOCCH_3)_4CO$, 102746-26-9; $Rh_2(OAc)_2(HNOCCH_3)_2CO$, 102746-27-0; $Rh_2(OAc)_4CO$, 102746-28-1; CO, 630-08-0.